DNA photoionization: from high to low energies

Evangelos Balanikas, Dimitra Markovitsi

3. DNA photoionization: from high to low energies

E. Balanikas and D. Markovitsi*

Université Paris-Saclay, CEA, CNRS, LIDYL, F-91191 Gif-sur-Yvette, France *

email address: dimitra.markovitsi@cea.fr

ABSTRACT

This Chapter discusses DNA photoionization in aqueous solution resulting from direct absorption of ultraviolet radiation. While DNA photoionization at wavelengths shorter than 200 nm was reported in the 1990s, recent studies showed that it also takes place at much longer wavelengths, with efficiencies depending strongly on the secondary structure. The quantum yield of one-photon ionization determined for duplex genomic DNA at 266 nm is $2x10^{-3}$ and significantly higher, reaching 10^{-2}, for guanine quadruplexes. The transient species issued from photoionization are studied by nanosecond flash photolysis from ~30 nanoseconds to 300 milliseconds. At this time-window, the ejected electrons are hydrated and the radicals are located on guanines or adenines. The quasi entire population of radical cations in genomic DNA undergoes deprotonation within 2 µs. Deprotonation in guanine quadruplexes is a highly anisotropic process, taking place from 30 ns to over 50 µs.

3.1 Introduction

Absorption of one or more UV photons directly by DNA may lead to its ionization: an electron is ejected generating an electron hole (radical cation) on the nucleic acid[1-3]. Subsequently, these primary species undergo a cascade of chemical transformations, which may ultimately damage DNA[4-6]. The transient species issued from the photoionization of various DNA systems, spanning from isolated bases in the gas phase to genomic DNA in aqueous solution, are studied by spectroscopic techniques using a large range of excitation wavelengths and detection methods.

Water molecules, which are key structural elements of DNA, are known to affect the photoionization process[7, 8] and interact with both electrons and radicals[9]. Therefore, this Chapter is dedicated to the photoionization of aqueous DNA solutions.

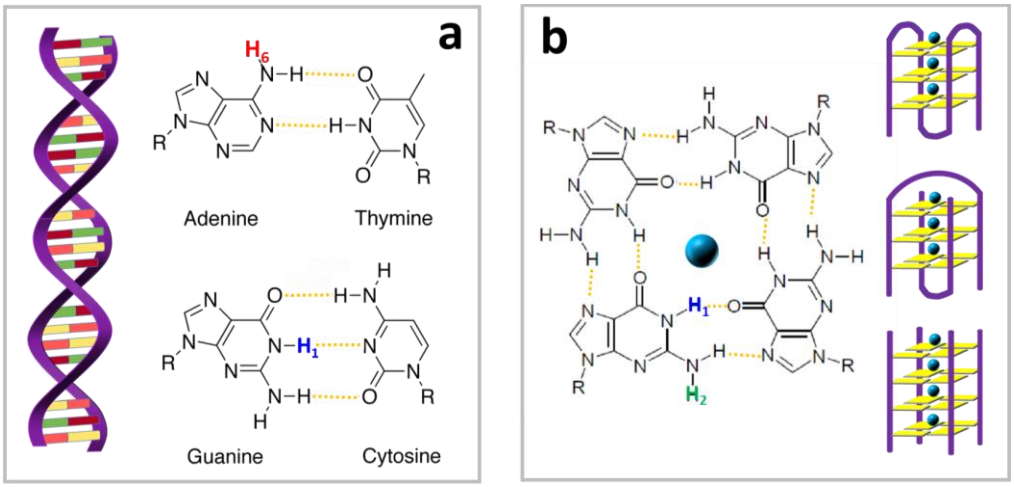

***Figure 1**. DNA structures whose low-energy photoionization has been studied[3]. (a) Duplexes composed of adenine-thymine and/or guanine cytosine base-pairs. (b) G-quadruplexes, characterized by vertical stacking of guanine tetrads (in yellow); they are formed by folding of a single DNA strand (monomolecular), association of two single strands (bimolecular) or association of four single strands (tetramolecular) in aqueous solution containing either Na^+ or K^+ cations (blue spheres). The phosphate deoxyribose backbone is indicated in violet. For simplicity, nucleobases at the loops, joining the guanine tetrads, and the ending groups have been omitted in (b). The red, blue and green protons are discussed in Section 3.5 in respect to the deprotonation of radical cations.*

In a first part (Section 3.2), we examine the mechanisms underlying one-photon ionization, because they are potentially involved in the damage provoked by the solar light, in contrast to multiphoton ionization, attained by intense lasers. We discuss the energies associated in this process, determined by photoelectron spectroscopy, and introduce the quantum yield ϕ_i, representing the probability of an ionization event per absorbed photon, determined by nanosecond flash photolysis. Those at high energy, 6.42 - 6.20 eV (193 - 200 nm), were mainly reported about 30 years ago[10-12]. More recently, a series of studies in our laboratory evidenced that, in the case of duplexes and guanine quadruplexes (G-quadruplexes), represented schematically in Figure 1, one-photon ionization is also operative at lower energies[3, 13] and determined ϕ_i values at 266 nm (4.66 eV). We also discuss the factors indicating that low-energy photoionization occurs via a different mechanism (indirect) from that involved in the high-energy process (direct).

In a subsequent section (3.3), we focus on the nanosecond flash photolysis. This time-resolved spectroscopic technique, in addition to the determination of ϕ_i mentioned above, allows the study of the transient species stemming from ionization. The latter are identified by their absorption spectra and quantified with respect to the number of absorbed photons. Their evolution is followed from the nanosecond to the millisecond time-scales, providing precious indications about possible reaction paths.

After examining the fate of ejected electrons (Section 3.4), we focus on purine radicals. Guanine is the nucleobase with the lowest oxidation potential[14]. Consequently, following a charge migration process[15-19], the electron hole finds itself on a guanine site. Nevertheless, in absence of guanines, the electron hole is trapped by adenines[13, 20]. In Section 3.5, we present the transformations that the adenine and guanine

radicals, stemming from photoionization, undergo during the time. We present the absorption spectra of the transient species and discuss changes observed when going from monomeric radicals to those in duplexes and G-quadruplexes. We show how the populations of various radical species at a given time are determined in respect to the ejected electrons. We also stress the anisotropic nature of the reactions taking place in DNA; for this reason, photoionization studies give a more reliable picture of the "intrinsic" radical reaction dynamics compared to methods using external oxidants, such as photosensitized electron abstraction[21].

Finally, we evoke the final lesions potentially resulting from photoionization (Section 3.6). In fact, the studies presented in this Chapter do not allow their characterization, which requires analytical chemistry methods. However, they provide information regarding their extent as well as the type of radicals responsible for them. These studies also explain the oxidative damage observed upon absorption of UVB/UVA radiation directly by DNA[22, 23].

3.2 Energies and quantum yields

3.2.1 Direct high-energy photoionization

Direct photoionization takes place when the photon energy is sufficiently high to detach an electron from the molecule; this energy corresponds to the ionization potential. Experimental ionization potentials (IP_{exp}) of DNA/RNA components in aqueous environment were reported only recently[24, 25]. They were determined for liquid jets combining synchrotron radiation and photoelectron spectroscopy. Photoelectron spectra were recorded between 6 and 10 eV and IP_{exp} values were derived from the band peaks. In parallel, IP were determined by quantum chemistry methods[8]. These theoretical studies showed that the IP_{exp} match the so-called Vertical

Ionization Potential (VIP) (Table 1), which correspond to electron detachment prior to any geometrical modification of the molecule accompanying the excited state relaxation. Computations also found that base-pairing and base-stacking have only a weak effect on VIPs, in line with the experimental finding that the photoelectron spectrum obtained for herring sperm DNA resembles that of an equimolar of the four constitutive mononucleotides[26].

Table 1. *Experimental Ionization Potentials (IP_{exp}) and computed lower Vertical Ionization Potentials (VIP) in eV, determined for DNA/RNA components in water by photoelectron spectroscopy and quantum chemistry calculations, respectively[25].*

	ribose	deoxyribose	dT	TMP	Cyt	CMP	Ado	$dAMP^-$	Guo	$dGMP^-$
IP_{exp}	9.4	9.4	-	8.1	8.1	-	7.6	7.7	7.3	-
VIP	9.2	9.1	7.9	7.8	7.8	7.8	7.7	7.7	7.4	7.1

DNA photoionization in solution is still observable at energies somewhat lower than the values in Table 1, where flash photolysis measurements are possible (Figure 2). Selected one-photon ionization quantum yields determined by this method with excitation at 193 nm (6.42 eV) are presented in Table 2.

Table 2. *One-photon ionization quantum yields (ϕ_i x10^3) determined at 193 nm (6.42 eV) for aqueous solutions.*

dT	dC	dA	dG/dGMP	CT-DNA[a]	$H_2PO_4^-/HPO_4^{2-}$	H_2O
55[11]	17[11]	24[11]	73/70[11]	36[1]/58[2]	330/520[11]	13[27]

a) *calf thymus DNA in water[1] and $NaClO_4$ aqueous solution[2]*

As found by photoelectron spectroscopy, the ϕ_i determined for duplex genomic DNA corresponds roughly to the average of the ϕ_i values found for its monomeric constituents suggesting that the same direct photoionization mechanism is operative.

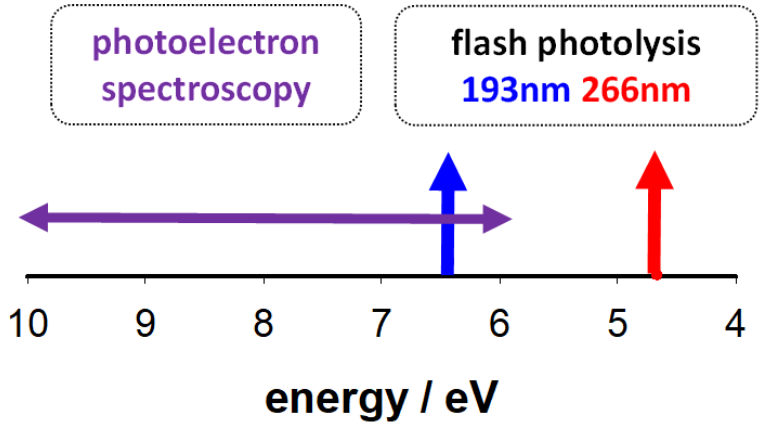

***Figure 2**. Energies corresponding to experimental studies of one-photon ionization of DNA in water: photoelectron spectra recorded between 10 and 6 eV (violet region); nanosecond flash photolysis measurements with excitation at 193 nm (blue arrow) and 266 nm (red arrow).*

3.2.2 Indirect low-energy photoionization

The ϕ_i values determined with excitation at 266 nm, are more than one order of magnitude smaller (Tables 3-5) than those obtained at 193 nm (Table 2). In contrast to what is observed for high-energy photoionization, the low-energy process strongly depends on the DNA secondary structure. While it is not detectable for mononucleotides and poorly stacked single strands (Table 3), the ϕ_i may be up to 30 times higher for well-structured DNA multimers.

Table 3. *One-photon ionization quantum yields (ϕ_i x10^3) determined at 266 nm / 4.66 eV for DNA single strands in phosphate buffer.*

$(A)_{20}$	$(T)_{20}$	5'-TTAGGG-3'	S1[a)]
1.1 ± 0.1^{28}	$<0.5^{13}$	$<0.3^{29}$	1.1 ± 0.3^{21}

a) *S1: 5'-CGTACTCTTTGGTGGGTCGGTTCTTTCTAT-3'*

Model duplexes containing twenty base-pairs of the same type in a repetitive sequence (homopolymeric adenine-thymine, alternating adenine-thymine or

alternating guanine-cytosine), exhibit quite similar ϕ_i, values, 1.0×10^{-3} - 1.5×10^{-3} (Table 4). If both types of base-pairs are present in a random sequence the ϕ_i increases by *ca*. 40% and remains practically the same, when going from a duplex with 30 base-pairs to a very long genomic DNA (2.0×10^{-3}). This suggests that rather the base sequence than the duplex size is a decisive parameter, as it will be discussed later.

Table 4. *One-photon ionization quantum yields (ϕ_i x10^3) determined at 266 nm / 4.66 eV for DNA duplexes in phosphate buffer.*

$(A)_{20}\bullet(T)_{20}$	$(AT)_{10}\bullet(AT)_{10}$	$(GC)_5\bullet(GC)_5$	S1•S2[a)]	CT-DNA[b)]
1.4 ± 0.1^{28}	1.1 ± 0.1^{20}	1.2 ± 0.2^{30}	2.1 ± 0.4^{21}	2.0 ± 0.2^{3}

[a)] *S1: 5'-CGTACTCTTTGGTGGGTCGGTTCTTTCTAT-3'; S2: 3'-GCATGAGAAACCACCCAGCCAAGAAAGATA-5';* [b)] *CT-DNA: calf thymus DNA.*

The propensity of G-quadruplexes to undergo low-energy photoionization is significantly larger compared to duplexes: not only their ϕ_i values are higher but also exhibit a more important dispersion, varying from 3.5×10^{-3} to 9.8×10^{-3} (Table 5). Such a dispersion arises from their structural diversity. Despite their common feature of vertically stacked guanine tetrads (Figure 1b), they contain additional loops joining the tetrads and/or dangling ends, whose length and/or base sequence vary from one system to the other. In addition, the metal cations (Na^+ or K^+) located in their central cavity are constitutive elements of these structures, contributing to their stability. Therefore, the type of cation is noted in their abbreviations in Table 5.

From the studies performed so far, it appears that the number of tetrads composing the G-quadruplex core does not play a role on their capacity to photo-eject an electron. For example, the ϕ_i of $(TG_4T)_4/Na^+$ with four tetrads (3.5×10^{-3}) is lower than that of TEL25/Na^+, characterized by three tetrads (5.2×10^{-3}). The same lack of correlation is observed in Table 5 between the ϕ_i values and the molecularity of the four-stranded

structure, *i.e.* the number of DNA strands that are associated together (Figure 1b). A small decrease of ϕ_i is detected when the dangling groups TA at the 5' end and TT at the 3' end are removed from the telomeric sequence (4.5×10^{-3} for TEL21/Na^+ vs 5.2×10^{-3} for TEL25/Na^+).

In contrast to the structural parameters mentioned above, the metal cations located in the central cavity of G-quadruplexes have a strong influence on their photoionization: for all the examined sequences the presence of K^+ leads to higher ϕ_i values compared to Na^+[31]. This behaviour is not encountered for duplex genomic DNA, whose ϕ_i remains the same when Na^+ ions are replaced by K^+ ions in the buffer in which it is dissolved[3].

Table 5. *One-photon ionization quantum yields (ϕ_i) determined at 266 nm / 4.66 eV for G-quadruplexes in phosphate buffer containing either Na^+ or K^+ cations.*

Type (Figure 1)	sequence	system	$\phi_i \times 10^3$	*reference*
Monomolecular	$TAGGG(TTAGGG)_3TT$	TEL25/$Na^{+a)}$	5.2 ± 0.3	21
	$GGG(TTAGGG)_3$	TEL21/$Na^{+\,a)}$	4.5 ± 0.6	29
		TEL21/$K^{+\,a)}$	9.4 ± 0.1	32
Bimolecular	GGGGTTTTGGGG	OXY/$Na^{+\,b)}$	6.0 ± 0.2	3
		OXY/$K^{+\,b)}$	7.9 ± 0.1	3
Tetramolecular	TGGGGT	$(TG_4T)_4/Na^+$	3.5 ± 0.5	33
		$(TG_4T)_4/K^+$	8.1 ± 0.5	31

[a)] *TEL: containing the human telomeric repeat TTAGGG* [b)]*OXY: containing the oxytricha nova telomeric repeat TTTTGGGG*

The ensemble of the results obtained for low-energy photoionization point toward a mechanism different than that underlying the high-energy process discussed in

previous section. This is further supported by quantum chemistry calculations performed for the tetramolecular G-quadruplexes $(TG_4T)_4/Na^+$ and $(TG_4T)_4/K^+$: the VIPs, computed for these two systems using the same computational method, differ less than 3%[31] while the their ϕ_i values vary by a factor of two (Table 5). On the basis of these studies, combined with the knowledge accumulated since the beginning of the 21st century on the relaxation of electronic excited states and charge transport in DNA (see Chapter 5), a complex indirect mechanism has been proposed to explain low-energy photoionization of DNA.

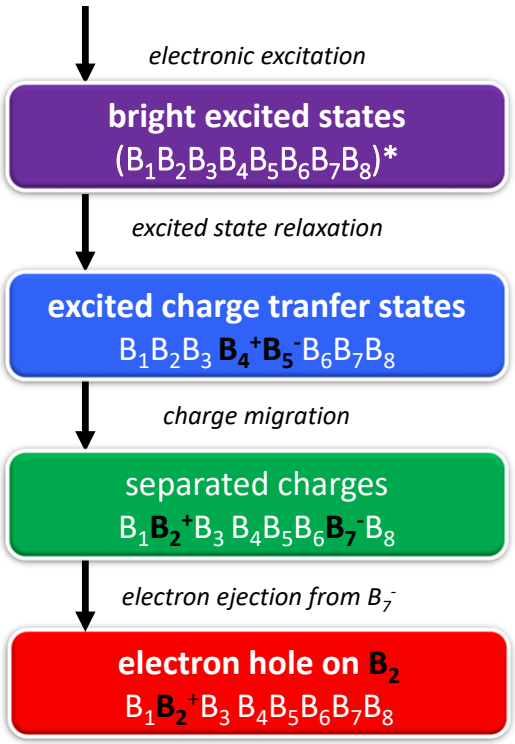

***Figure 3**. Successive steps potentially leading to DNA photoionization at low-energies. B_i designate stacked nucleobases.*

The main steps of the proposed mechanism are schematically depicted in Figure 3. Initially, photon absorption populates excited states which may be delocalized over a few nucleobases. Very rapidly, an important part of the excited state population evolves toward excited charge transfer states, in which negative and positive charges

are located on adjacent stacked nucleobases. These “charged” nucleobases normally undergo a geometrical rearrangement, including modification in their solvation, so that to minimize their energy, and, subsequently, they recombine to the ground state. However, it is possible that, prior to such a modification, a small part of the excited charge transfer states undergoes charge separation[34]. As the VIP of “anionic” nucleobases is lower than that of “neutral” ones[35], electron ejection may take place from the negatively charged moiety under the effect of conformational motions, leaving an electron hole at some other part of the system.

A key step of this mechanism is charge migration leading to charge separation[34]. The higher propensity of G-quadruplexes to undergo low-energy photoionization compared to duplexes is attributed to trapping of the positive charge by the guanine core, potentially accompanied by charge delocalization[36, 37], while the negative charge may be located on a nucleobase of a loop or an ending group. The presence in their central cavity of Na^+ ions, which are smaller and more mobile that K^+ ions, favour geometrical stabilization of the excited charge transfer states and, consequently, charge migration to neighbouring nucleobases becomes less effective, leading to lower ϕ_i values.

Although duplexes are devoid of such distinct structural elements, GG or GGG steps are known to behave as traps for electron holes[38, 39], the charge separation being ensured by conformational motions. Thus, it is understandable that S1:S2 and calf thymus DNA, which contain such traps, have higher ϕ_i values than duplexes with simpler repetitive base sequence (Table 4).

3.3 Nanosecond flash photolysis: advantages and limitations

Before discussing the evolution of various transient species issued from photoionization, we present the basic concept of such measurements. Although the

general lines employed for experiments with low-energy excitation were inspired from older studies with high-energy excitation, we put emphasis on the more recent ones, which profited from technical and methodological improvements and allowed the study of several duplexes and G-quadruplexes.

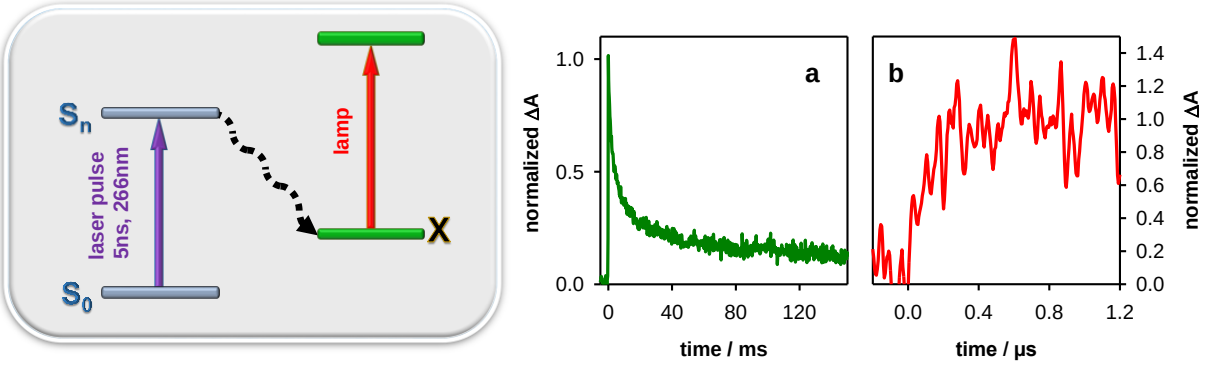

Figure 4*. Left panel: schematic representation of flash photolysis measurements. Right panel: examples of transient absorption signals obtained for TEL25/Na^+ at 500 nm[21] (a; decay) and TEL21/K^+ at 620 nm[32] (b; rise).*

Flash photolysis is a time-resolved absorption technique (Figure 4). DNA is excited by a nanosecond laser pulse. Absorption of the laser photons leads, among others, to the formation of a transient species X. Its presence in the solution is probed with the help of a lamp allowing the determination of differential absorbance, corresponding the difference in the absorbance before and after the excitation: $\Delta A = A_{after} - A_{before}$. As X is unstable, its ΔA decreases with the time (Figure 4a). If, instead, X is formed during the time-window of the observation, a rise is detected (Figure 4b).

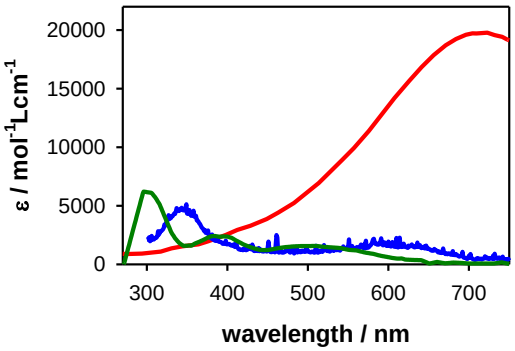

***Figure 5**. Comparison of the absorption spectra of ejected electrons (red; e_{hyd}^- [40]) and the corresponding holes on adenine (blue; dA[28]) and guanine (green: dGMP[41]) moieties.*

Although several transient species may co-exist in photoexcited DNA, the knowledge of their absorption spectra helps disentangling them. It is well-established that electrons ejected in aqueous solution become hydrated within a few picoseconds[42]; the spectrum of hydrated electrons e_{hyd}^- is characterized by a large absorption band peaking at 720 nm (Figure 5)[40] and extending all over the whole visible spectral domain. The absorption of radical cations located on adenines or guanines, whose spectra are also shown in Figure 5, is very weak compared to that of e_{hyd}^-. Their relatively intense UV bands cannot be exploited because they may interfere with the absorption of both DNA[28, 29] and dimeric phototoproducts[20, 43, 44] (see Chapter 2). Consequently, the radical cations and the subsequent deprotonated radicals (see Section 3.5.1) can be properly detected only when e_{hyd}^- have decayed.

Figure 6 illustrates the time-domains on which nanosecond flash photolysis provides information about the transient species issued from photoionization. Due to a time-resolution of 30 ns, all the steps related with complex mechanism depicted in Figure 3 are not accessible. Their direct observation, which could unambiguously validate the proposed mechanism, is a real challenge. As a matter of fact, femtosecond setups,

254 which have appropriate time-resolution, experience difficulties in detecting transient
255 species corresponding to only 10^{-3} of the excited state population.

256 The ΔA signals determined around 700 nm provide the lifetime of e_{hyd}^-, which, under
257 the conditions used in these experiments, disappear within a few microseconds
258 (Figure 6 in red). However, their decays become faster in presence of efficient
259 scavengers (O_2, NO_3, N_2O…), rendering possible the study of nucleobase radicals
260 over a larger time window (see for example Figure 4b). We note that, because of
261 technical reasons, the sensitivity of the method is smaller at shorter times. The
262 nucleobase radicals decay completely on the millisecond time-scale (Figure 6 in
263 green).

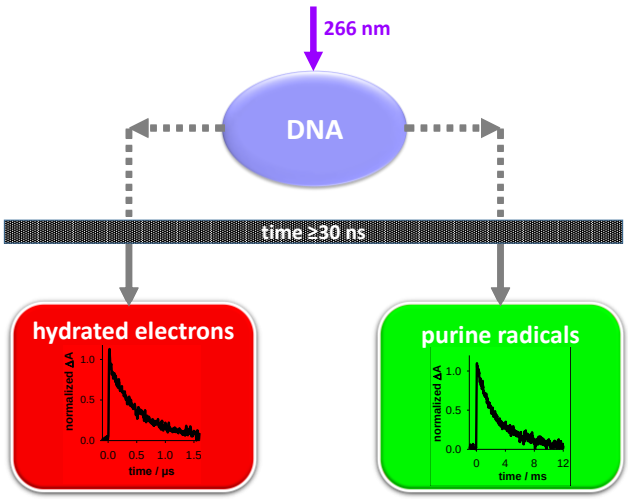

264

265 ***Figure 6***. *Schematic illustration of the time-domains on which nanosecond flash photolysis provides*
266 *information about the transient species issued from DNA photoionization. As examples are given the*
267 *decays of* e_{hyd}^- *and adenine radicals determined for alternating adenine-thymine duplexes*[20].

268

269 These experiments are not only performed with low-energy excitation but also using
270 low-intensity laser pulses to circumvent saturation effects, as explained in detail in
271 reference[3]. As a result, the transient absorption signals are very weak, requiring long
272 measurements in order to reduce the signal-to-noise ratio. In addition, frequent

replacement of the DNA solutions is indispensable so that to avoid exciting the DNA that has been already damaged. This condition, associated to the importance of using purified nucleic acids, makes such studies particularly long and expensive.

3.4 Evolution of ejected electrons

We already pointed out that the only form of electrons observable by nanosecond flash photolysis is the hydrated one, which disappears within a few microseconds. In fact, their lifetime depends on the molecules present in the solution. In most of the experiments on low-energy photoionization, DNA is dissolved in phosphate buffer composed of an equimolar mixture of MH_2PO_4 and M_2HPO_4 (M = Na^+ or K^+) in concentrations of 0.15 mol·L^{-1} each, which is four orders of magnitude higher than the concentration of model DNA systems. It is well-known that $H_2PO_4^-$ ions react with e_{hyd}^- ($e_{hyd}^- + H_2PO_4^{2-} \rightarrow H^{\bullet} + HPO_4^{2-}$ [45]). This reaction takes indeed place in the case of the reported experiments as attested by the variation of the e_{hyd}^- decay with the buffer concentration (Figure 7).

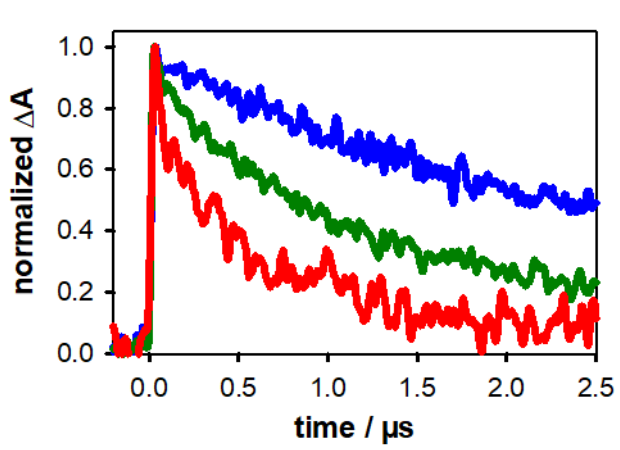

***Figure 7**. Photoionization of CT-DNA: variation of the e_{hyd}^- decay with the concentration of $H_2PO_4^-$ ions; 0.15 mol·L^{-1} (red), 0.015 mol·L^{-1} (green) and 0 (DNA dissolved in ultrapure water: blue).*

The decays of e_{hyd}^- stemming from oligomeric DNA systems can be described by mono-exponential functions. The lifetimes derived from the fits are independent of the type of the studied system, depending only on the buffer concentration (0.5 µs in usual conditions). Such a behaviour means that the reaction with $H_2PO_4^-$ ions constitutes by far the dominant reaction path. Incidentally, the high concentration of the phosphate buffer used in these studies protects DNA from being attacked by e_{hyd}^- [6].

The situation changes when going from model systems to genomic DNA. In this case, the lifetime of e_{hyd}^- becomes significantly shorter than those observed for oligomeric structures[3]. In addition, it can no more be described by a mono-exponential functions. Hence, it was deduced that additional reaction paths, involving the DNA itself, are also operative. Their occurrence was explained by the flexibility of the very long natural macromolecule[46] which could facilitate the encounter between components of the nucleic acid and e_{hyd}^- that are generated in their vicinity.

3.5. Evolution of purine radicals

3.5.1 Deprotonation and tautomerization

Adenine and guanine radical cations, $(A^+)^\bullet$ and $(G^+)^\bullet$, are stronger acids than the parent nucleobases. Consequently, when they are generated in neutral aqueous solution they tend to lose a proton[11] (see Figure 1). For dAMP, the proton at position 6 (H6) is transferred to the bulk water, giving rise to the deprotonated radical $(A\text{-}H6)^\bullet$. In the case of dGMP, the loss of the proton at position 1 (H1) leads to the formation of the $(G\text{-}H1)^\bullet$ deprotonated radical. The spectra of these deprotonated radicals have been determined by high-energy photo-ionization and/or using oxidizing agents (Figures 8a and 8b)[11, 41]. They exhibit only subtle differences from those of the

314 corresponding radical cations (Figure 5), obtained in low temperature glasses[17] or in
315 pH 3[14], where deprotonation is avoided.

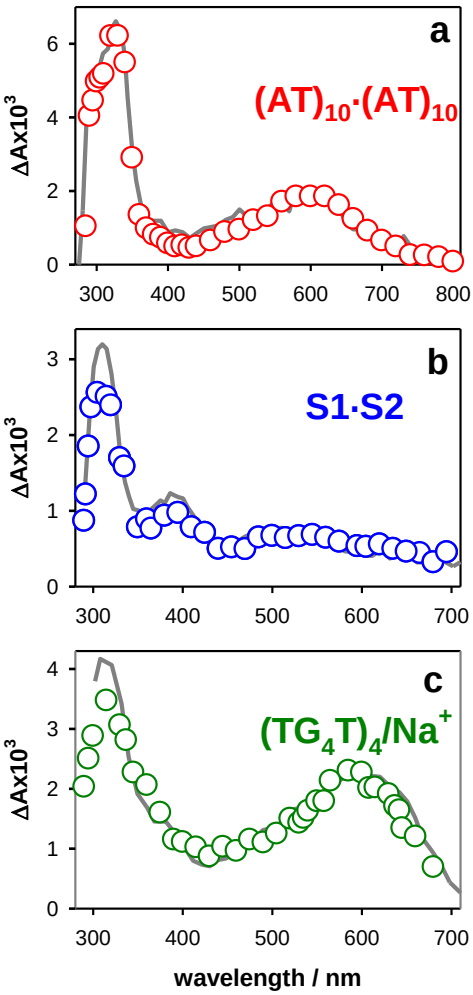

316

317 ***Figure 8***. *Comparison of the transient absorption spectra obtained for DNA multimers (circles) with*
318 *those of monomeric deprotonated radicals (grey lines): $(AT)_{10}$•$(AT)_{10}$ duplex at 200 μs[20] and (A-H6)•* [11]*
319 (a); S1•S2 duplex (see Table 4) at 5 μs[21] and (G-H1)•* [11] *(b); $(TG_4T)_4/Na^+$ G-quadruplex at 50 μs[33] and*
320 *(G-H2)•* [47]*. The intensity of monomeric radical spectra has been arbitrarily normalized to that of the*
321 *corresponding multimer.*

322

323 As the H6 proton of adenine is not perturbed by base-pairing, deprotonation in
324 duplexes is expected to lead also to (A-H6)•. This is attested by the perfect overlap of

the spectra obtained for dAMP and $(AT)_{10}$•$(AT)_{10}$ following high-energy[11] and low-energy photoionization[20], respectively (Figure 8a).

Guanine deprotonation in duplexes and G-quadruplexes is more complex because the H1 proton is engaged in hydrogen bonding (Figure 1). In duplexes, the H1 proton may be transferred either to cytosine or to the bulk water[1]; quantum chemistry calculations on GC pairs showed that the absorption spectra of the resulting deprotonated radicals exhibit only weak differences[31]. A bigger spectral modification is observed if the H2 proton is lost[31]. Absorption spectra of $(G\text{-}H2)^{\bullet}$ deprotonated radicals were determined experimentally by flash photolysis and pulse radiolysis experiments on monomeric guanine derivatives[41, 47] (Figure 8c).

The transient absorption spectra recorded for both model duplexes[21, 30] and genomic DNA[3] by low-energy photoionization strongly resemble those of the monomeric $(G\text{-}H1)^{\bullet}$ in the visible spectral domain (Figure 8b). It is possible that the radicals corresponding to H1 proton transferred to the cytosine were missed due the insufficient time-resolution and/or the poor sensitivity of the measurements.

A completely different picture emerged for deprotonation of guanine radical cations in G-quadruplexes. In agreement with the results obtained by photosensitized electron abstraction from these systems[48], photoionization studies revealed the formation of $(G\text{-}H2)^{\bullet}$ radicals[3, 21, 29, 32, 33] (Figure 8c). In most cases, $(G^{+})^{\bullet} \rightarrow (G\text{-}H2)^{\bullet}$ deprotonation is followed by $(G\text{-}H2)^{\bullet} \rightarrow (G\text{-}H1)^{\bullet}$ tautomerization[3, 29, 33]. These findings were rationalized by quantum chemistry calculations showing that $(G\text{-}H2)^{\bullet}$ radicals in G-quadruplexes are more stable than $(G\text{-}H1)^{\bullet}$ [33]. In addition, theoretical studies found that the general features of the guanine radical spectra are maintained within four-stranded structures[49].

3.5.2 Radical populations

The spectral similarity of the various deprotonated radicals of purines in duplexes and G-quadruplexes with those determined for their monomeric analogues, allows their quantification. This is achieved via the Beer Lambert law, using the molar absorption coefficients ε determined for the monomeric species in the visible spectral domain[11]. Moreover, the spectra recorded following photoionization of G-quadruplexes in pH 3 match, in the 450-700 nm domain, the spectrum of monomeric $(G^{+})^{\bullet}$ both in shape and in intensity[3].

The quantification of the radical population in duplexes is straightforward, as only one type of deprotonated radical is detected in these systems at times ≥ 3μs (Figures 8a and 8b). In contrast, two or three types of radicals may coexist in G-quadruplexes. In this case, the total radical population is determined considering that at 510-515 nm the ε of $(G^{+})^{\bullet}$, $(G\text{-}H2)^{\bullet}$ and $(G\text{-}H1)^{\bullet}$ is the same[3]. Subsequently, the transient absorption spectra of G-quadruplexes are reconstructed as a linear combinations of the corresponding monomeric spectra and the population of each type of radical is determined[3, 32].

Following the above methodology, it was found that the radical population in all the examined duplexes and G-quadruplexes at 3 μs equals that of the hydrated ejected electrons; the associated error, depending on the system, was estimated to be lower than 5%. A straightforward conclusion is that no major reaction besides deprotonation takes place before 3 μs.

3.5.3 Reaction dynamics

The decays of the radical population in DNA multimers span over at least four orders of magnitude of time. Although they can be described by multi-exponential functions, it is not appropriate to assign the time-constants derived from such fits to specific species. The reason is that radical formation and/or decay underlie bimolecular reactions taking place in a highly anisotropic space. For example, deprotonation of radical cations involves water molecules whose approach to the reactive site depends on its location. Under these conditions, the kinetic models developed for reactions in homogenous solutions are not valid[43,44]. It should be noted that other processes, such as DNA fluorescence[50] or solvation[51, 52] in DNA multimers also undergo multiscale dynamics.

Given the above described difficulty, the radical reaction dynamics in various DNA multimers was simply compared by considering their half-life ($\tau_{1/2}$), *i.e.* the time at which the entire radical population has decreased by a factor 2. For all the examined systems $\tau_{1/2}$ amounts to a few milliseconds.[3] Base-pairing slows down the radical decays, with $\tau_{1/2}$ increasing, for example, from 1 to 4 ms for adenine tracts[28]. Such a change in the reaction rate is explained by the higher degrees of freedom characterizing single strands compared to duplexes, allowing deprotonated radicals to reach faster reactive conformations, and their larger exposure to water. In G-quadruplexes, the $\tau_{1/2}$ values depend strongly on the type of the metal cations located in their central cavity: they are at least twice as high for Na^+ compared to K^+, but the mechanism responsible for such different dynamics is not yet clear.

Focusing on the deprotonation dynamics occurring before 2 µs, a few delicate photoionization experiments, using electron scavengers (N_2O or NO_3^-), provided information for guanine radicals. Thus, a rise of transient absorption was observed (Figure 4) at wavelengths at which the absorbance of deprotonated radicals is more intense than that of $(G^+)^\bullet$ [3, 32]. Hence, it was found that deprotonation in calf thymus-DNA is completed within 2 µs[3]. A faster deprotonation process, occurring in less than 1 µs, was detected for TEL21/K^+ and OXY/K^+. But this rapid step concerns only part of the $(G^+)^\bullet$ population in G-quadruplexes which ranges from 40% to 75%, depending on the system. The remaining part of $(G^+)^\bullet$ survives in G-quadruplexes for much longer times, at least several tens of microseconds.

The decays of deprotonated radicals are not affected neither by the presence of oxygen nor by the buffer ingredients. Consequently, the associated reactions should involve only the nucleic acid itself and/or water molecules. Under these conditions, the decays represent, in a certain way, the “intrinsic” radical reaction dynamics, which can be obtained only via low-energy/low-intensity excitation, triggering solely DNA photoionization. In contrast, high-energy photoionization generates also electrons from the aqueous solvent (Table 2) which are known to react nucleic acids[9] altering the transient absorption signals.

The time evolution of nucleobase radicals has been largely studied by flash photolysis and pulse radiolysis, using electron abstraction mediated by other molecules. According to these methodologies, a laser pulse or a pulsed electron beam triggers a redox reaction between the DNA and an external oxidant. Although such studies have brought important insights, in particular regarding the deprotonation of electron holes[48, 53, 54], they fail to correctly describe radical dynamics over long time-scales[21].

This happens because they involve bimolecular reactions requiring the approach between an oxidant, such as $SO_4^{-\bullet}$, and the DNA, which is an anionic polyelectrolyte with a highly inhomogeneous structure. As a result, the generation of radicals may interfere with their decay, artificially changing their reaction dynamics. A detailed comparison of guanine radical reaction dynamics in duplexes and G-quadruplexes obtained by an external oxidant[55, 56] and low-energy photoionization is presented in reference 21.

3.6 Final lesions

Although the studies presented in this Chapter concern the primary species issued from photoionization, they provide some information regarding the associated final DNA damage. The total quantum yield of the final lesions ϕ_t resulting from purine radicals, irrespectively of their nature, should be equal to the ϕ_i at the irradiation wavelength. Additional damage may also be provoked via reactions involving e_{hyd}^-. The existence of two different photoionization mechanisms (direct and indirect) shows that such DNA damage may be provoked by irradiation over a large spectral domain. Starting from 180 nm, ϕ_t should decrease with increasing wavelength, in line with the behaviour of direct ionization[24, 26]. Then, upon reaching the absorption band peaking at 260 nm, where the indirect process takes over, a non-monotonous variation is expected. In this case, radical generation depends only on the formation of excited charge transfer states, which is the main relaxation path in DNA multimers (see Chapter 5). It should even be extended over the UVA spectral domain, where DNA exhibits a weak absorption tail[57, 58], correlated with excited states having partial charge transfer character[59, 60]. The wide spectral efficiency of low-energy photoionizaion is corroborated by the detection of DNA lesions stemming from guanine radicals after

UVB[22] and even UVA[23] irradiation. Despite a few efforts to characterize specific lesions resulting from one-photon ionization of DNA at either high- or at low-energies[22, 29, 61], the determined quantum yields were significantly lower than ϕ_t, meaning that an important part of final lesions remained unidentified.

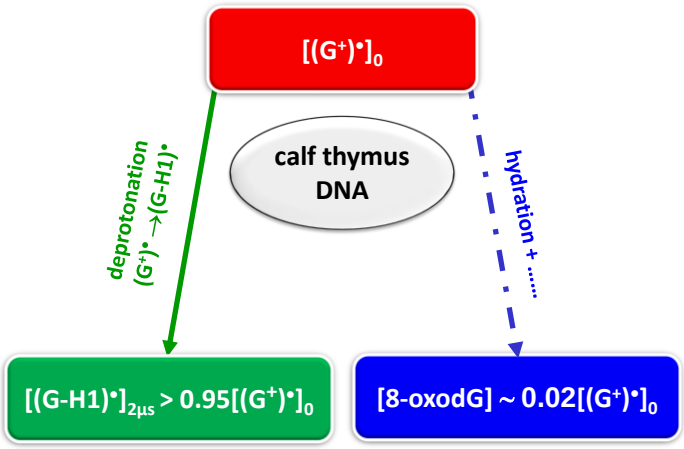

***Figure 9**. Competition between two reactions involving guanine radical cations: deprotonation and hydration, ultimately leading the formation of 8-oxodG.*

A second important outcome of the time-resolved studies on DNA photoionization concerns the interplay between dynamics and populations. In other terms, if there is competition between two reactions, the most important part of the reactant population evolves along the faster path. This is illustrated in Figure 9 for two reactions involving $(G^+)^\bullet$: on the one hand deprotonation and, on the other, hydration which ultimately leads to formation of 8-oxo-7,8-dihydro-2′-deoxyguanosine (8-oxodG)[62]. In the case of calf thymus DNA, deprotonation is a fast reaction, being completed within 2 µs; at this time the quasi-entire $(G^+)^\bullet$ population (>95%) has been transformed to deprotonated $(G\text{-}H1)^\bullet$ radicals. Thus, it is not surprising that the quantum yield determined for the formation of 8-oxodG by analytical methods corresponds only 2% of the ϕ_t [22]. In

contrast, as part of $(G^{+})^{\bullet}$ survives in TEL21/Na^{+} for longer times, a higher level of 8-oxodG (corresponding to 7% of the ϕ_i) has been detected for this G-quadruplex[29]. The corollary is that 8-oxodG, widely used as marker of oxidative damage, is not representative of the extent of this damage when it takes place by one electron oxidation leading to the formation of radical cations.

Under the above conditions, the great majority of oxidative lesions are expected to stem from deprotonated radicals. The fact that the radical decays are not sensitive versus oxygen shows that neither imidazolone nor oxazolone constitute major lesions since their formation requires aerated conditions[63]. In contrast, oxygen does not affect strand breakage. As a matter of fact, strand breakage was detected following both 193 nm irradiation[2, 61] and UVA irradiation[23].

The reactions involving $(G\text{-}H2)^{\bullet}$, which represents the only deprotonated radical in some G-quadruplexes, have never been explored. Yet, the fingerprint of a reaction intermediate has been observed in the transient absorption spectra of TEL21/K^{+} around 350-450 nm[32]. Finally, the role of metal cations in the central cavity of G-quadruplexes, which affect the radical reaction rate, needs also to be assessed.

ACKNOWLEDGMENT

This work has received funding from the European Union's Horizon 2020 research and innovation programme under the Marie Sklodowska-Curie grant agreement No. 765266 (LightDyNAmics).

References

1. L. P. Candeias, P. Oneill, G. D. D. Jones and S. Steenken, *Int. J. Radiat. Biol.*, 1992, **61**, 15-20.
2. T. Melvin, M. A. Plumb, S. W. Botchway, P. Oneill and A. W. Parker, *Photochem. Photobiol.*, 1995, **61**, 584-591.

3. E. Balanikas, A. Banyasz, T. Douki, G. Baldacchino and D. Markovitsi, *Acc. Chem. Res.*, 2020, **53**, 1511-1519.
4. G. G. Gurzadyan, R. K. Ispiryan and K. S. Voskanyan, *J. Photochem. Photobiol. B-Biol.*, 1991, **11**, 269-275.
5. J. Cadet and K. J. A. Davies, *Free Radical Biology and Medicine*, 2017, **107**, 2-12.
6. A. Kumar, D. Becker, A. Adhikary and M. D. Sevilla, *Int. J. Mol. Sci.*, 2019, **20**.
7. O. T. Ehrler and D. M. Neumark, *Acc. Chem. Res.*, 2009, **42**, 769-777.
8. E. Pluharova, P. Slavicek and P. Jungwirth, *Acc. Chem. Res.*, 2015, **48**, 1209-1217.
9. S. Steenken, *Chem. Rev.*, 1989, **89**, 503-520.
10. M. Wala, E. Bothe, H. Görner and D. Schulte-Frohlinde, *J. Photochem. Photobiol. A-Chem.*, 1990, **53**, 87-108.
11. L. P. Candeias and S. Steenken, *J. Am. Chem. Soc.*, 1992, **114**, 699-704.
12. T. Melvin, S. W. Botchway, A. W. Parker and P. Oneill, *J. Am. Chem. Soc.*, 1996, **118**, 10031-10036.
13. S. Marguet, D. Markovitsi and F. Talbot, *J. Phys. Chem. B*, 2006, **110**, 11037-11039.
14. E. Palecek and M. Bartosik, *Chem. Rev.*, 2012, **112**, 3427-3481.
15. B. Giese, J. Amaudrut, A.-K. Köhler, M. Spormann and S. Wessely, *Nature*, 2001, **412**, 318-320.
16. S. Kanvah, J. Joseph, G. B. Schuster, R. N. Barnett, C. L. Cleveland and U. Landman, *Acc. Chem. Res.*, 2010, **43**, 280-287.
17. J. C. Genereux and J. K. Barton, *Chem. Rev.*, 2010, **110**, 1642-1662.
18. K. Kawai and T. Majima, *Acc. Chem. Res.*, 2013, **46**, 2616-2625.
19. F. D. Lewis, R. M. Young and M. R. Wasielewski, *Acc. Chem. Res.*, 2018, **51**, 1746-1754.
20. A. Banyasz, T. Ketola, L. Martinez-Fernandez, R. Improta and D. Markovitsi, *Faraday Disc.*, 2018, **207**, 181-197.
21. E. Balanikas, A. Banyasz, G. Baldacchino and D. Markovitsi, *Molecules*, 2019, **24**, 2347.
22. M. Gomez-Mendoza, A. Banyasz, T. Douki, D. Markovitsi and J. L. Ravanat, *J. Phys. Chem. Lett.*, 2016, **7**, 3945-3948.
23. J. Teychene, D. Didacus-Prins, N. Chouini-Lalanne, V. Sartor and C. Dejugnat, *J. Mol. Liq.*, 2019, **295**, 111712.
24. P. Slavicek, B. Winter, M. Faubel, S. E. Bradforth and P. Jungwirth, *J. Am. Chem. Soc.*, 2009, **131**, 6460-6467.
25. C. A. Schroeder, E. Pluharova, R. Seidel, W. P. Schroeder, M. Faubel, P. Slavicek, B. Winter, P. Jungwirth and S. E. Bradforth, *J. Am. Chem. Soc.*, 2015, **137**, 201-209.
26. E. Pluharova, C. Schroeder, R. Seidel, S. E. Bradforth, B. Winter, M. Faubel, P. Slavicek and P. Jungwirth, *J. Phys. Chem. Lett.*, 2013, **4**, 3766-3769.
27. D. M. Bartels and R. A. Crowell, *J. Phys. Chem. A*, 2000, **104**, 3349-3355.
28. A. Banyasz, T. Ketola, A. Muñoz-Losa, S. Rishi, A. Adhikary, M. D. Sevilla, L. Martinez-Fernandez, R. Improrta and D. Markovitsi, *J. Phys. Chem. Lett.*, 2016, **7**, 3949-3953.
29. A. Banyasz, L. Martinez-Fernandez, C. Balty, M. Perron, T. Douki, R. Improta and D. Markovitsi, *J. Am. Chem. Soc.*, 2017, **139**, 10561-10568.
30. A. Banyasz, L. Martinez-Fernandez, R. Improta, T. M. Ketola, C. Balty and D. Markovitsi, *Phys. Chem. Chem. Phys.*, 2018, **20**, 21381-21389.
31. B. Behmand, E. Balanikas, L. Martinez-Fernandez, R. Improta, A. Banyasz, G. Baldacchino and D. Markovitsi, *J. Phys. Chem. Lett.*, 2020, **11**, 1305−1309.
32. E. Balanikas, A. Banyasz, G. Baldacchino and D. Markovitsi, *Molecules*, 2020, **25**, 2094.
33. A. Banyasz, E. Balanikas, L. Martinez-Fernandez, G. Baldacchino, T. Douki, R. Improta and D. Markovitsi, *J. Phys. Chem. B*, 2019, **123**, 4950-4957.
34. D. B. Bucher, B. M. Pilles, T. Carell and W. Zinth, *Proc. Natl. Acad. Sci. USA*, 2014, **111**, 4369-4374.
35. J. Schiedt, R. Weinkauf, D. M. Neumark and E. W. Schlag, *Chem. Phys.*, 1998, **239**, 511-524.

36. W. M. Sun, D. Varsano and R. Di Felice, *Nanomaterials*, 2016, **6**.
37. L. Martinez-Fernandez, A. Banyasz, D. Markovitsi and I. Improta, *Chem. Europ. J.*, 2018, **24**, 15185-15189.
38. E. Meggers, M. E. Michel-Beyerle and B. Giese, *J. Am. Chem. Soc.*, 1998, **120**, 12950-12955.
39. I. Saito, T. Nakamura, K. Nakatani, Y. Yoshioka, K. Yamaguchi and H. Sugiyama, *J. Am. Chem. Soc.*, 1998, **120**, 12686-12687.
40. F. Torche and J. L. Marignier, *J. Phys. Chem. B*, 2016, **120**, 7201-7206.
41. L. P. Candeias and S. Steenken, *J. Am. Chem. Soc.*, 1989, **111**, 1094-1099.
42. Y. Gauduel, A. Migus, J. P. Chambaret and A. Antonetti, *Rev. Phys. Appl.*, 1987, **22**, 1755-1759.
43. S. Marguet and D. Markovitsi, *J. Am. Chem. Soc.*, 2005, **127**, 5780-5781.
44. A. Banyasz, L. Martinez-Fernandez, T. Ketola, A. Muñoz-Losa, L. Esposito, D. Markovitsi and R. Improta, *J. Phys. Chem. Lett.*, 2016, **7**, 2020-2023.
45. in *Free-Radical-Induced DNA Damage and Its Repair: A Chemical Perspective*, Springer Berlin Heidelberg, Berlin, Heidelberg, 2006, pp. 77-86.
46. D. R. Tree, A. Muralidhar, P. S. Doyle and K. D. Dorfman, *Macromolecules*, 2013, **46**, 8369-8382.
47. C. Chatgilialoglu, C. Caminal, A. Altieri, G. C. Vougioukalakis, Q. G. Mulazzani, T. Gimisis and M. Guerra, *J. Am. Chem. Soc.*, 2006, **128**, 13796-13805.
48. L. D. Wu, K. H. Liu, J. L. Jie, D. Song and H. M. Su, *J. Am. Chem. Soc.*, 2015, **137**, 259-266.
49. L. Martinez-Fernandez, L. Esposito and R. Improta, *Photochem. Photobiol. Sci.*, 2020, **19**, 436-444.
50. T. Gustavsson and D. Markovitsi, *Acc. Chem. Res.*, 2021, **54**, 1226-1235.
51. D. Andreatta, J. L. Pérez Lustres, S. A. Kovalenko, N. P. Ernsting, C. J. Murphy, R. S. Coleman and M. A. Berg, *J. Am. Chem. Soc.*, 2005, **127**, 7270-7271.
52. S. Mukherjee, S. Mondal, S. Acharya and B. Bagchi, *J. Phys. Chem. B*, 2018, **122**, 11743-11761.
53. K. Kobayashi and S. Tagawa, *J. Am. Chem. Soc.*, 2003, **125**, 10213-10218.
54. K. Kobayashi, R. Yamagami and S. Tagawa, *J. Phys. Chem. B*, 2008, **112**, 10752-10757.
55. Y. Rokhlenko, J. Cadet, N. E. Geacintov and V. Shafirovich, *J. Am. Chem. Soc.*, 2014, **136**, 5956-5962.
56. T. J. Merta, N. E. Geacintov and V. Shafirovich, *Photochem. Photobiol.*, 2019, **95**, 244-251.
57. J. C. Sutherland and K. P. Griffin, *Radiat. Res.*, 1981, **86**, 399-410.
58. S. Mouret, C. Philippe, J. Gracia-Chantegrel, A. Banyasz, S. Karpati, D. Markovitsi and T. Douki, *Org. Biomol. Chem.*, 2010, **8**, 1706–1711.
59. A. Banyasz, I. Vayá, P. Changenet-Barret, T. Gustavsson, T. Douki and D. Markovitsi, *J. Am. Chem. Soc.*, 2011, **133**, 5163-5165.
60. V. A. Spata and S. Matsika, *J. Phys. Chem. A*, 2014, **118**, 12021-12030.
61. T. Melvin, M. A. Plumb, S. W. Botchway, P. Oneill and A. W. Parker, *The distribution of single strand breakage at guanine initiated by 193nm light is different for single and double stranded DNA*, 1995.
62. J. Cadet, T. Douki and J. L. Ravanat, *Acc. Chem. Res.*, 2008, **41**, 1075-1083.
63. J. L. Ravanat, T. Douki and J. Cadet, *J. Photochem. Photobiol., B: Biology*, 2001, **63**, 88-102.